



**HAL**  
open science

## Steady-State Voltage Modelling of a HT-PEMFC under Various Operating Conditions

Sylvain Rigal, Amine Jaafar, Christophe Turpin, Théophile Hordé,  
Jean-Baptiste Jollys, Paul Kreczanik

► **To cite this version:**

Sylvain Rigal, Amine Jaafar, Christophe Turpin, Théophile Hordé, Jean-Baptiste Jollys, et al.. Steady-State Voltage Modelling of a HT-PEMFC under Various Operating Conditions. *Energies*, 2024, 17 (3), pp.573. 10.3390/en17030573 . hal-04837181

**HAL Id: hal-04837181**

**<https://hal.science/hal-04837181v1>**

Submitted on 13 Dec 2024

**HAL** is a multi-disciplinary open access archive for the deposit and dissemination of scientific research documents, whether they are published or not. The documents may come from teaching and research institutions in France or abroad, or from public or private research centers.




L'archive ouverte pluridisciplinaire **HAL**, est destinée au dépôt et à la diffusion de documents scientifiques de niveau recherche, publiés ou non, émanant des établissements d'enseignement et de recherche français ou étrangers, des laboratoires publics ou privés.



Distributed under a Creative Commons Attribution 4.0 International License

## Article

# Steady-State Voltage Modelling of a HT-PEMFC under Various Operating Conditions

Sylvain Rigal <sup>1,2</sup> , Amine Jaafar <sup>2,\*</sup> , Christophe Turpin <sup>2</sup>, Théophile Hordé <sup>3</sup>, Jean-Baptiste Jollys <sup>4</sup> and Paul Kreczanik <sup>1</sup> 

<sup>1</sup> Institute of Technology Saint Exupéry (IRT Saint Exupéry), 3 Rue Tarfaya, 31400 Toulouse, France; srigal.consulting@gmail.com (S.R.); paul.kreczanik@irt-saintexupery.com (P.K.)

<sup>2</sup> LAPLACE—Laboratoire Plasma et Conversion d'énergie Université de Toulouse, CNRS—Centre National de la Recherche Scientifique, INPT—Institut National Polytechnique de Toulouse, UPS—Université Paul Sabatier, 31077 Toulouse, France; christophe.turpin@laplace.univ-tlse.fr

<sup>3</sup> Airbus, 31703 Blagnac, France; theophile.horde@airbus.com

<sup>4</sup> Alstom, 50 Rue du Dr Guinier, 65600 Séméa, France; jean-baptiste.jollys@alstomgroup.com

\* Correspondence: amine.jaafar@laplace.univ-tlse.fr

**Abstract:** In this work, a commercially available membrane electrode assembly from Advent Technology Inc., developed for use in high-temperature proton exchange membrane fuel cells, was tested under various operating conditions (OCs) according to a sensibility study with three OCs varying on three levels: hydrogen gas over-stoichiometry (1.05, 1.2, 1.35), air gas over-stoichiometry (1.5, 2, 2.5), and temperature (140 °C, 160 °C, 180 °C). A polarization curve (V-I curve) was performed for each set of operating conditions (27 V-I curves in total). A semi-empirical and macroscopic (0D) model of the cell voltage was developed in steady-state conditions to model these experimental data. With the proposed parameterization approach, only one set of parameters is used in order to model all the experimental curves (simultaneous optimization with 27 curves). Thus, an air over-stoichiometry-dependent model was developed. The obtained results are promising between 0.2 and 0.8 A·cm<sup>-2</sup>: an average error less than 1.5% and a maximum error around 7% between modeled and measured voltages with only 9 parameters to identify. The obtained parameters appear consistent, regardless of the OCs. The proposed approach with only one set of parameters seems to be an interesting way to converge towards the uniqueness of consistent parameters.

**Keywords:** fuel cells; high temperature proton exchange membrane (HT-PEMFC); hydrogen; mathematical model; steady-state model



**Citation:** Rigal, S.; Jaafar, A.; Turpin, C.; Hordé, T.; Jollys, J.-B.; Kreczanik, P. Steady-State Voltage Modelling of a HT-PEMFC under Various Operating Conditions. *Energies* **2024**, *17*, 573. <https://doi.org/10.3390/en17030573>

Academic Editors: Yanzhou Qin, Yulin Wang and Xiao Ma

Received: 14 December 2023

Revised: 12 January 2024

Accepted: 19 January 2024

Published: 24 January 2024



**Copyright:** © 2024 by the authors. Licensee MDPI, Basel, Switzerland. This article is an open access article distributed under the terms and conditions of the Creative Commons Attribution (CC BY) license (<https://creativecommons.org/licenses/by/4.0/>).

## 1. Introduction

Despite the significant lack of data regarding the global impact of a “hydrogen economy” and its relevance in terms of “sustainable development” [1], fuel cells currently hold great hope as an alternative to actuators using fossil fuels. The use of fuel cells for aeronautical applications is proposed as one of the technological solutions in order to decarbonize this sector, responsible for 2–6% of the global radiative forcing of human activity [2]. Fuel cells based on Nafion<sup>®</sup> (or equivalent perfluorosulfonic acid polymer), i.e., Low Temperature Proton Exchange Membrane Fuel Cells (LT-PEMFCs), show interesting performance for terrestrial applications. However, LT-PEMFCs suffer from (i) a complex water management [3], (ii) a low fuel impurity tolerance (carbon monoxide and hydrogen sulfide) [4,5], (iii) a difficult cooling in the case of embedded applications exposed to relatively high ambient temperatures [3], and (iv) a hardly exploitable heat production because the operating temperature is lower than 100 °C (373.15 K) [3]. This technology is currently the subject of an intensive research effort, which makes these drawbacks less and less problematic and makes LT-PEMFC one of the most interesting technologies for embedded applications (with air as an oxidant). As an example, we can cite recent advances in the

efficiency of cooling systems [6,7]. Furthermore, we can also cite recent progress on bipolar plates in order to increase the power density of the LT-PEMFC stack, such as Hycco<sup>®</sup>'s composite technology, which makes it possible to increase the stack power density by 18% and expect to achieve a more than 80% increase in 2024 [8].

Nevertheless, it should be noted that all these disadvantages could be reduced by increasing the operating temperature of LT-PEMFCs. Nevertheless, the operating temperature of LT-PEMFCs cannot be effortlessly increased due to the properties of the membrane (used as an electrolyte). Indeed, the LT-PEMFC membrane needs liquid water to reach sufficient proton conductivity [9]. Furthermore, irreversible degradations of the membrane (polymer chain breaking) occur at temperatures above 90 °C (363.15 K), which results in insufficient mechanical integrity and proton conductivity [10]. In order to operate at higher temperatures, the most common alternative to Nafion<sup>®</sup> (or equivalent) is the phosphoric acid doped PolyBenzImidazole (PBI), which results in a High-Temperature PEMFC (HT-PEMFC) operating typically around 160 °C (433.15 K) [11]. (in the following sections, the term "HT-PEMFC" will refer to this last technology using doped PBI as an electrolyte.)

Compared to LT-PEMFCs, this technology benefits from (i) all the benefits of high temperatures (take the opposite of all the LT-PEMFC drawbacks above), (ii) a simplified operation (dry gases and atmospheric pressure), (iii) a more stable voltage due to the absence of liquid water, and to insist on this advantage (iv) an easier cooling at higher ambient temperatures. This could be a real advantage for transport applications with an ambient temperature higher than 40 °C, such as an aircraft in the tarmac of an airport in an arid zone. As a matter of fact, it could significantly reduce the weight and volume of the cooling system compared to LT technology, which is critical for aeronautical applications, for example. However, there is no published work addressing the relevance of PBI-based HT-PEMFC in aeronautical applications, to the best of the authors' knowledge. In comparison to LT-PEMFCs, the HT technology suffers from (i) a longer start-up due to an unavoidable pre-heating process to limit the acid pumping (by acid dissolution in liquid water), which takes place when the phosphoric acid is in contact with liquid water; (ii) a loss of the corrosive electrolyte in normal operation [12]; and (iii) a lower lifetime, especially if metallic bipolar plates are used because of higher temperatures and more frequent contact with liquid acid [13]. It must be noticed that the main degradations observed with commercially available BASF MEAs are the catalyst particle growth and the corrosion of the electrodes, which is the major degradation during the test, including several starts and stops without appropriate experimental procedures [14]. After many years of development, there is no effective technological solution yet (the only partial workaround is to try to avoid potential excursions in the electrodes, as much as possible, by operational methods, for example, purging with an inert gas during shutdown). More generally, (iv) the HT-PEMFC suffers from a lower technological readiness level, TRL (medium TRL compared to high TRL for the LT-PEMFC [15]). It must be noticed that, recently, a promising new type of fuel has been presented by Tang H. et al. [16] working between −20 °C and 200 °C and could combine both the benefits of LT-PEMFC and HT-PEMFC.

However, the work presented in this paper will deal with the modeling of the technology using PBI doped with phosphoric acid, which has already reached industrial membrane electrode assembly (MEA) production. Steady-state voltage modeling of LT and HT-PEMFCs has been extensively studied to date [17,18]. A major analytic model of the impact of the stoichiometric ratio on LT-PEMFC performance was first proposed by A.A. Kulikovskiy [19]. However, this model requires good knowledge of several parameters related to the different MEAs layers, which are not always accessible with a commercially available MEA. The excess oxygen ratio has been modeled by several research teams [20,21] and exploited for modeling and control at the system level. Control-oriented models based on the description of physical phenomena evolved during fuel cell operation have been developed [22–25]. Because of the non-linearity and complexity of these models, "data-driven" modeling methods (neural network, support vector machine, and partial least squares) have been increasingly used for control-oriented modeling, taking into account

the oxygen ratio [26–29]. With HT-PEMFC, the impact of operating conditions (OCs) on cell performance was also significantly studied with the use of a large variety of models (pseudo-2D, 3D [30–32]). The remarkable stability of the voltage at high current densities compared to LT-PEMFC (probably due to the absence of liquid water) encourages us to develop a simple one-dimensional and empirical model of the air stoichiometry impact on the cell voltage at the macroscopic level. Such a model would make it possible to obtain rapid results while allowing a dissociation of the various losses within the MEA, which then facilitates the interpretation of the physical phenomena impacting the quasi-static performances. However, the analytic zero-dimensional (0D) model, air over-stoichiometry-dependent, is still non-existent in the HT-PEMFC literature, to our knowledge.

In this work, a commercially available HT-MEA (Advent Technologies Inc., Boston, MA, USA) using a phosphoric acid-doped PBI membrane was tested in 27 different OCs according to a sensibility study with three parameters varying on three levels: hydrogen ( $H_2$ ) gas over-stoichiometry ( $\lambda_{H_2}$ ), air gas over-stoichiometry ( $\lambda_{air}$ ), and temperature ( $T$ ). The experimental part is first presented. Then, experimental results will be shown in the next part, and afterwards, an original air over-stoichiometry-dependent model and the parameterization approach will be described. Finally, model validation and its predictive ability will be discussed.

## 2. Experimental Setup

The tested MEAs were manufactured by Advent Technologies Inc.-Boston, MA, USA, model PBI MEA (formerly BASF P1100W), and operated thanks to a BASF single cell module (commercially available).

The cell temperature management was ensured through successive cooling and heating phases, achieved respectively by two external fans and two electrical resistances (160 W each) located on each external face of the end plates (Figures 1 and 2 give a picture of the single cell module and the flow-field plates (two parallel serpentine flow fields for the anode and three parallel for the cathode side), respectively).

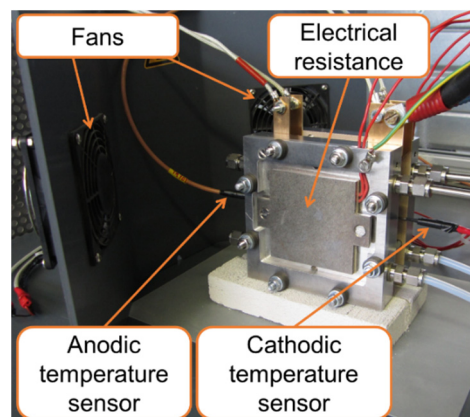


Figure 1. Picture of the fuel cell module from BASF installed in the test bench.

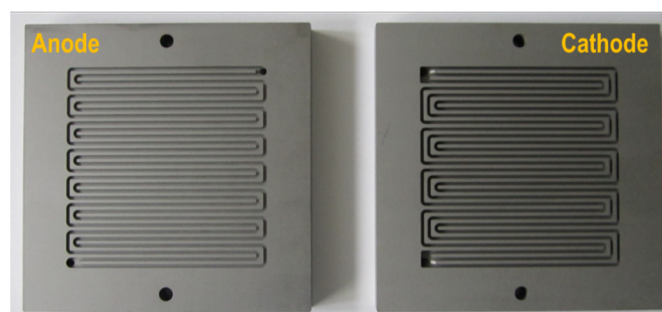


Figure 2. Picture of the graphite flow field plates of the fuel cell module from BASF.

After any assembly of the single-cell module and after each start of the test bench, a start-up procedure was applied. This procedure is fully detailed in [33]. The break-in procedure for the fresh MEA was carried out for approximately 50 h at nominal conditions: 160 °C (433.15 K), 0.2 A·cm<sup>-2</sup> (cell area: 45 cm<sup>2</sup>),  $\lambda_{H_2} = 1.2$ ,  $\lambda_{air} = 2$ , dry gases, and atmospheric pressure (gas exhausts at the atmosphere). After the break-in period, a sensibility study with three parameters varying on three levels was carried out. The pressure was not controlled, and the gas exhausts were in the atmosphere for all tests. The three varied factors of the sensibility study are hydrogen gas over-stoichiometry ( $\lambda_{H_2}$ ), air gas over-stoichiometry ( $\lambda_{air}$ ) and temperature ( $T$ ). Their ranges of values are presented in Table 1. The goal of this study was to estimate the impact of these three parameters on performance. The medium value of the OCs are the “nominal” OCs recommended by the manufacturer. The minimum values were chosen in order to obtain a range of OCs achievable in a real industrial fuel cell system in a real application. The total number of combinations for the OCs is equal to 27 ( $3^3 = 27$ ). It took 14 days to perform all tests and approximately 210 h for the sensibility study (including overnight operation at nominal COs). For each set of OCs tested, a polarization curve was obtained by varying the cell current density from 1.1 A·cm<sup>-2</sup> to 0 A·cm<sup>-2</sup> over 22 current levels (including a measurement at Open Circuit Voltage, OCV); see “v(i)\_3” on Figure 5 in [34] for an illustration of the current variation used. For each level, the current was maintained constant for one minute, which was assumed to be sufficient to tend towards the steady state (with a current density variation lower than 0.2 A·cm<sup>-2</sup> between two consecutive stages). However, the first stage at 1.1 A·cm<sup>-2</sup> was prolonged for 15 minutes in order to tend towards the steady state because the current density varied from 0.2 A·cm<sup>-2</sup> to 1.1 A·cm<sup>-2</sup> before this stage, which corresponds to a higher variation compared to the one performed between two consecutive stages during the polarization curve. Between two consecutive current stages, the current varied with a current slope of approximately 2.2 mA·cm<sup>-2</sup>·s<sup>-1</sup>. It has to be noted that the minimal flow rates adjustable on the used test bench were 0.33 cm<sup>3</sup>·s<sup>-1</sup> (at Standard Conditions for Temperature and Pressure, SCTP, defined as a temperature of 273.15 K and an absolute pressure of exactly 101.325 kPa) for H<sub>2</sub> and 1.33 cm<sup>3</sup>·s<sup>-1</sup> (at SCTP) for air (corresponding to a current density of 0.05 A·cm<sup>-2</sup> with  $\lambda_{H_2} = 1.2$  and  $\lambda_{air} = 2$ ). Thus, the gas over-stoichiometries increased when the current density decreased below 0.05 A·cm<sup>-2</sup> (with  $\lambda_{H_2} = 1.2$  and  $\lambda_{air} = 2$ ), whereas they were maintained constant above this current density (therefore for most part of the polarization curve).

**Table 1.** Variation range for the three varied parameters of the sensibility study.

Parameter Symbol	Minimum Value	Medium Value	Maximum Value
$\lambda_{H_2}$	1.05	1.2	1.35
$\lambda_{air}$	1.5	2	2.5
$T$	140 °C (413.15 K)	160 °C (433.15 K)	180 °C (453.15 K)

In this work, all physical quantities (voltage, current, temperatures, flow rates, etc.) related to a “point” of a polarization curve plot are taken as the average value of the 10 last measurements (corresponding to the 10 last seconds) at the end of each one-minute stage during the polarization curve acquisition. Furthermore, after these 10 s, if the current is above or equal to 0.022 A·cm<sup>-2</sup>, successive sinusoidal currents at successive frequencies of around 0.044 A·cm<sup>-2</sup> amplitude peak-to-peak were superimposed on the cell current in order to perform an Electrochemical Impedance Spectroscopy (EIS) measurement. The EIS was performed between 20 kHz and 1 Hz (which takes approximately 2 min) with a Diagnostack (EIS analyzer) from Alstom Hydrogène SAS, Aix En Provence, France. EIS results are not presented in this work except for the High Frequency Impedance which is used to model the ohmic resistance of the cell.

When no characterizations were performed (including overnight), the test bench was not stopped, and the cell was left at nominal conditions: 160 °C (433.15 K), 0.2 A·cm<sup>-2</sup>,  $\lambda_{H_2} = 1.2$ ,  $\lambda_{air} = 2$ , dry gases, and atmospheric pressure.

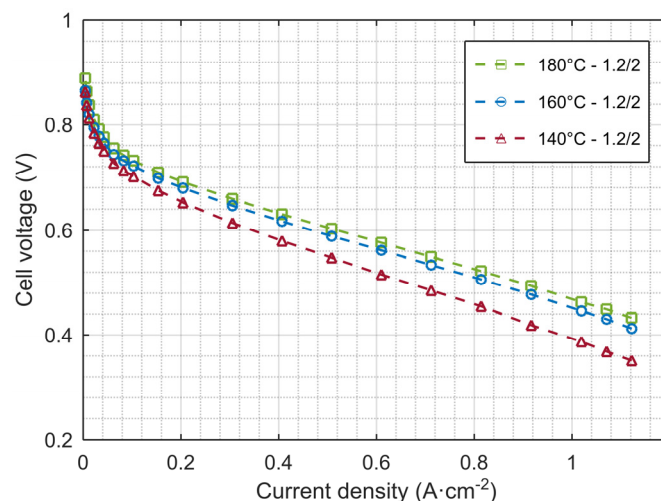
When the temperature was modified during the sensibility study (each time starting from the nominal conditions), the stabilization of temperature was reached during the first increase in the current (from 0.2 A·cm<sup>-2</sup> to 1.1 A·cm<sup>-2</sup> during approximately 409 s) and a wait of 15 min at 1.1 A·cm<sup>-2</sup>.

It must be noted that the cell experiences voltage degradation during this sensibility study. This degradation was estimated by performing a polarization curve (called the reference VI curve) at nominal conditions (i.e., medium values given in Table 1) between each characterization (i.e., between each VI curve of the sensibility study: 27 curves). A reference VI curve was obtained in the same way as a VI curve of the sensibility study except with regard to the current decrease, which was made by imposing a current slope of 0.003 A·cm<sup>-2</sup>·s<sup>-1</sup> to the cell from 1.1 to 0.2 A·cm<sup>-2</sup>. At the end of the whole campaign, there are more reference VI curves than the VI curve of the sensibility study because a reference VI curve was acquired at the beginning and at the end of every day of experimentation. At the end, 40 reference VI curves were obtained after 14 days of testing.

This voltage loss is estimated to be around 7% at 1.1 A·cm<sup>-2</sup> at the end of the sensibility study (after the last VI curve of the sensibility study) compared to the beginning (before the first VI curve of the sensibility study). The impact of this degradation on the modeling results will be briefly discussed in Section 5.

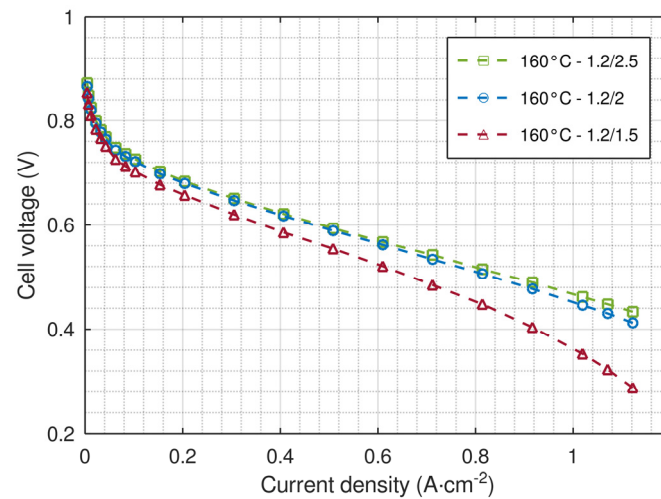
### 3. Experimental Results

Figure 3 shows polarization curves obtained during the sensibility study at different operating temperatures. As expected, a significant impact of operating temperature on performance is observed (at 1.1 A·cm<sup>-2</sup>, compared to 160 °C, 5% higher performance at 180 °C, and 15% lower at 140 °C).



**Figure 3.** Experimental cell voltages of the polarization curve at  $\lambda_{H_2}/\lambda_{air} = 1.2/2$  and different operating temperatures: 140 °C ( $\Delta$ ), 160 °C (o), and 180 °C ( $\square$ ) obtained during a sensibility study.

Figure 4 shows the polarization curves obtained during the sensibility study at different air over-stoichiometry. A significant impact of air over-stoichiometry on performance is observed (at 1.1 A·cm<sup>-2</sup>, compared to  $\lambda_{air} = 2$ , 5% higher performance at  $\lambda_{air} = 2.5$  and 30% lower at  $\lambda_{air} = 1.5$ ), but a saturation effect is present above  $\lambda_{air} = 2$  and current density is lower than approximately 0.6 A·cm<sup>-2</sup>. However, hydrogen over-stoichiometry shows negligible impact compared to air over-stoichiometry or temperature (see Figure 5). Figure 5 shows 9 polarization curves, 3 curves for each operating temperature corresponding to the 3 different  $\lambda_{H_2}$  values tested (at constant  $\lambda_{air}$ ). The maximum impact of  $\lambda_{H_2}$  at a given temperature is around  $\pm 1$  mV, which corresponds to the measurement uncertainty.



**Figure 4.** Experimental cell voltages of the polarization curve at 160 °C,  $\lambda_{H_2} = 1.2$ , and different  $\lambda_{air}$ : 1.5 ( $\Delta$ ), 2 (o), and 2.5 ( $\square$ ) obtained during a sensibility study.

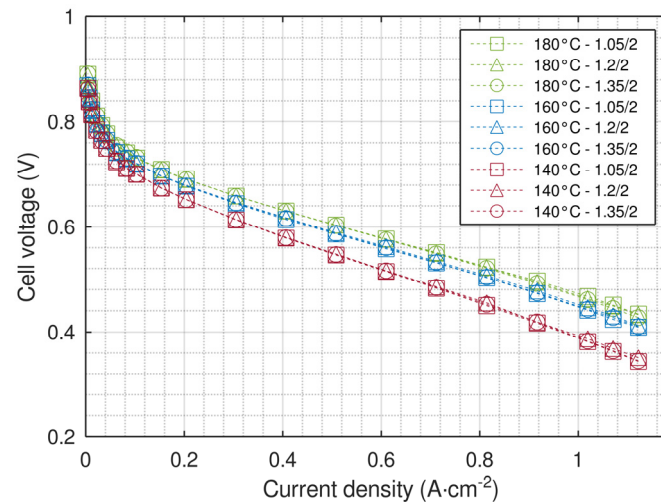


**Figure 5.** Experimental cell voltages of the polarization curve at  $\lambda_{air} = 1.2$ , different  $\lambda_{H_2}$ —1.05 ( $\square$ ); 1.2 ( $\Delta$ ); and 1.35 (o)—and different operating temperatures—140 °C (red); 160 °C (blue); and 180 °C (green).

Thanks to these experimental observations, it has been chosen to model only the impact of  $\lambda_{air}$  and operating temperature on steady-state cell voltage. The model used will be presented in the following section.

#### 4. Model Development

The basis of the semi-empirical and macroscopic models used here was first proposed by Guillaume Fontès et al. [35] and completed by Isabelle Labach et al. [36] for LT-PEMFCs (this model will be mentioned as the “Basic Model” in the following sections). The fine description and validation of this Basic Model are described in previous work [37], but only the governing equations are given here. This is a theoretical prediction (0D, i.e., no computation of fluid flow), isothermal, and steady-state model of the cell voltage.

A first validation of this Basic Model was published in [37]. In this work, the model is improved in order to integrate the dependence on air over-stoichiometry and perfect the temperature dependence because, as we saw in Figure 5, only these two parameters have a significant impact on the cell voltage among the 3 tested parameters in the sensibility study, i.e., temperature, air, and H<sub>2</sub> over-stoichiometry.

#### 4.1. Basic Model

##### 4.1.1. Governing Equations

The model of the cell voltage ( $U_{cell}$ ) is given by Equation (1) [33,37]:

$$U_{cell} = E_{rev} - \eta_{act} - \eta_{ohm} - \eta_{diff} \quad (1)$$

with,

$$E_{rev} = -\frac{\Delta G^0}{n \cdot F} + \frac{R \cdot T}{n \cdot F} \ln(p_{H_2} \cdot p_{O_2}^{1/2}) \quad (2)$$

$$\eta_{act} = \frac{RT}{\alpha n F} \ln\left(\frac{j_{cell}}{j_0}\right) \quad (3)$$

$$\eta_{ohm} = R_{cell} \cdot j_{cell} \quad (4)$$

$$\eta_{diff} = -\frac{RT}{\beta n F} \ln\left(1 - \frac{j_{cell}}{j_{lim}}\right) \quad (5)$$

The names of each parameter in the above equations are given as follows, and some of them are listed in Table 2 with more details: in Equation (1),  $E_{rev}$  is the reversible voltage of the cell,  $\eta_{act}$  is the voltage drop due to “activation losses” (due to charge-transfer processes and simply called “activation losses” in the following sections),  $\eta_{ohm}$  is the voltage drop due to “ohmic losses” (due to the total resistance of the cell including ionic, electronic, and contact resistances, and simply called “ohmic losses” in the following sections), and  $\eta_{diff}$  is the voltage drop due to “diffusion losses” (due to mass-transfer processes and simply called “diffusion losses” in the following sections). In Equation (2),  $\Delta G^0$  is the standard free enthalpy of water formation,  $n$  the number of exchanged electrons,  $F$  the faraday constant,  $R$  the ideal gas constant,  $T$  the operating temperature of the cell, and  $p$  the partial pressures of hydrogen or oxygen in the gas channels at steady-state conditions. In Equation (3),  $j_{cell}$  is the cell current density,  $j_0$  the exchange current density, and  $\alpha$  the charge transfer coefficient. In Equation (4),  $R_{cell}$  is the total resistance of the cell measured by EIS (at current where no EIS were performed, i.e., under  $0.022 \text{ A} \cdot \text{cm}^{-2}$ , the  $R_{cell}$  is considered constant and equal to the one measured at  $0.022 \text{ A} \cdot \text{cm}^{-2}$ ), and in Equation (5),  $j_{lim}$  is the diffusion limiting current density, and  $\beta$  the diffusion factor, introduced empirically [35].

**Table 2.** List of model parameters. A parameter subject to change with OCs or current is called Variable (measured or calculated), a parameter assumed to be constant is called Constant (measured or taken from literature), and a parameter used to fit the model with experimental data are called Fitting Parameter, which could depend (one parameter per VI curve) or not (one parameter for all VI) on OCs.

Parameter	Type	Value
$\Delta G^0$	Variable	Calculated
$n$	Constant	2
$F$	Constant	$96,485 \text{ C} \cdot \text{mol}^{-1}$
$R$	Constant	$8.314 \text{ J} \cdot \text{mol}^{-1} \cdot \text{K}$
$T$	Variable	Measured
$p_{H_2}$	Constant	Measured: 102,100 Pa absolute
$p_{O_2}$	Constant	Measured: 21,400 Pa absolute
$j_{cell}$	Variable	Measured
$j_0$	Fitting Parameter	OCs dependent
$\alpha$	Fitting Parameter	non-OCs dependent
$R_{cell}$	Variable	Measured
$j_{lim}$	Fitting Parameter	OCs dependent
$\beta$	Fitting Parameter	non-OCs dependent

It has to be noticed that Equation (3) is only valid if the exchange current density is negligible compared to the cell current (Tafel approximation of the Butler–Volmer equation [37]).



In this work, the exchange current density is in the range of  $10^{-5}$ – $10^{-6}$   $\text{A}\cdot\text{cm}^{-2}$  (cf. [37]), which is far from the minimum currents modeled here, i.e., higher than  $5 \times 10^{-3}$   $\text{A}\cdot\text{cm}^{-2}$ . In other words, the OCV, or more exactly, the range of extremely low current densities, including zero current, was not modeled in this work. This choice was also motivated by the fact that operating at OCV is prohibited with HT-PEMFC in order to limit carbon corrosion, which is accelerated with temperature increases [38].

#### 4.1.2. Model Validation

The model validation was implemented by fitting the model to experimental data using a parameter identification algorithm (fully presented in [37]) in order to minimize the error between the modeled and measured voltages, employing the Covariance Matrix Adaptation Evolution Strategy (CMA-ES) optimizer.

This identification process is applied simultaneously to all polarization curves (called the “multi-VI” approach), i.e., all OCs. Some parameters are supposed to be common to all curves ( $\alpha$  and  $\beta$ ) and some parameters to be different for each curve ( $j_0$  and  $j_{lim}$ ). At the end, with the 27 curves of the sensibility study (see Table 1), there are only one parameter  $\alpha$ , one parameter  $\beta$ , 27 parameters  $j_0$ , and 27 parameters  $j_{lim}$ , which gives a total of 56 parameters. In other words, it is assumed that only the parameters  $j_0$  and  $j_{lim}$  are influenced by the variation of OCs.

The parameter  $\alpha$  is assumed to be only dependent on the nature of the catalyst and, thus, independent of the OCs in the range explored. For platinum,  $\alpha$  is classically fixed to 0.5 for LT-PEMFCs [36]. This parameter is left free; here we are in the poorly known case of HT-PEMFCs.

The parameter  $\beta$  is linked to the reaction mechanism (via the order of reaction) [36] and assumed to be independent of the OCs explored.

It is finally assumed that  $\alpha$  and  $\beta$  were not impacted by the degradation of the cell during the tests (this degradation, around 7% loss at  $1.1 \text{ A}\cdot\text{cm}^{-2}$ , will be discussed in Section 5).

The identification method previously described and using 56 parameters was applied in [37]. The overall error obtained was 0.72%. This error is calculated in two steps: (i) The average error for all 22 current levels for each polarization curve is calculated. That gives 27 errors. (ii) Second, the average of these 27 errors is calculated as the overall error of the fitting. The maximum error at a given current level ( $0.7 \text{ A}\cdot\text{cm}^{-2}$ ) is about 2.55%, and it corresponds to the curve at  $180 \text{ }^\circ\text{C} - \lambda_{\text{H}_2/\text{air}} = 1.35/1.5$ . The parameters identified show satisfying consistency with the literature [37].

However, the use of this model requires the identification of four parameters per curve. Thus, it is useful for modeling existing data but not for predicting the behavior of the voltage in non-tested OCs. To address this limit, the model will be improved in this work in order to include an air over-stoichiometry dependency and a better temperature dependency. In this way, only one set of parameters common to all polarization curves will allow for modeling the voltage in the entire OCs domain explored.

### 4.2. Air Over-Stoichiometry Dependent Model

In order to obtain an air over-stoichiometry-dependent model, we will focus on two parameters that are assumed to be predominantly affected by OC variations, namely  $j_0$  and  $j_{lim}$ .

#### 4.2.1. Exchange Current Density Model

Equation (6) is commonly used for modeling the temperature dependency of  $j_0$  [39]. This equation was used in [37] for modeling the 27  $j_0$  obtained after the parameter identification described in Section 4.1.2, and the results were consistent (to perform this modeling,

the parameters  $E_a$  and  $i_{O,ref}$  were identified by fitting Equation (6) to the 27 previously obtained values of  $j_0$  for each air over-stoichiometry  $\lambda_{air}$ .

$$j_0 = \frac{i_{0,ref}}{S_{cell}} \left( \frac{p_{O_2}^*}{P_{ref}} \right)^\gamma \exp \left\{ -\frac{E_a}{RT} \left( 1 - \frac{T}{T_{ref}} \right) \right\} \quad (6)$$

where  $i_{0,ref}$  is the reference exchange current (temperature free and identified parameter),  $S_{cell}$  is the geometric area of the MEA (45 cm<sup>2</sup>),  $\gamma$  is the reaction order (identified parameter),  $p_{O_2}^*$  the oxygen partial pressure on the catalyst layer of the electrode,  $P_{ref}$  the reference pressure (1 atm absolute),  $E_a$  is the activation energy of the reaction (identified parameter),  $T$  is the operating temperature of the cell, and  $T_{ref}$  is the reference temperature (set here to 160 °C i.e., 433.15 K).

The air over-stoichiometry dependence is introduced in the model by correcting the partial pressure of oxygen in the gas channels ( $p_{O_2} = 21,400$  Pa absolute) through adding an empiric coefficient ( $coef_{\lambda_{air}}$ , to identify) in order to estimate the partial pressure in the catalyst layer of the electrode ( $p_{O_2}^*$ ), as it is shown in Equation (7) (in order to keep the model simple, a linear dependency on  $\lambda_{air}$  was tested and retained because of the interesting result obtained).

$$p_{O_2}^* = \frac{p_{O_2} \cdot \lambda_{air}}{coef_{\lambda_{air}}} \quad (7)$$

By substituting Equation (7) in Equation (6), we obtain Equation (8), an original semi-empirical model of  $j_0$ , temperature and  $\lambda_{air}$  dependent. The only parameters to identify for modeling 27  $j_0$  are  $\gamma$ ,  $E_a$ ,  $i_{O,ref}$ , and  $coef_{\lambda_{air}}$ . This identification gives a global error of 6.69% and a maximum error (for one  $j_0$ ) of 18.2%.

$$j_0 = \frac{i_{O,ref}}{S_{cell}} \left( \frac{p_{O_2} \cdot \lambda_{air}}{P_{ref} \cdot coef_{\lambda_{air}}} \right)^\gamma \exp \left\{ -\frac{E_a}{RT} \left( 1 - \frac{T}{T_{ref}} \right) \right\} \quad (8)$$

Parameter consistency is difficult to evaluate because Equation (6) is not often used in LT-PEMFC modeling and is never used in HT-PEMFC, to our knowledge. Compared to some data obtained in LT-PEMFC,  $\gamma = 0.45$ , which is near the reaction order for Oxygen Reduction Reaction (ORR) found in the literature: 0.37 to 0.52 [40] (p. 202), 0.54 [41], 0.56 [42], and 0.5 [32,43]. The parameter  $E_a = 8.2 \times 10^4$  J·mol<sup>-1</sup> is in the same order of magnitude compared to some LT-PEMFC results ( $5.8 \times 10^4$  J·mol<sup>-1</sup> to  $6.6 \times 10^4$  J·mol<sup>-1</sup> [40] (p. 202),  $6.7 \times 10^4$  J·mol<sup>-1</sup> [41]). Identical observations are made concerning  $i_{0,ref} = 3.89 \times 10^{-4}$  A ( $5.25 \times 10^{-5}$  A,  $4.50 \times 10^{-4}$  A, and  $4.85 \times 10^{-4}$  A [40] (p. 203)). The parameter  $coef_{\lambda_{air}} = 8.25$  is not present in the literature; it was introduced in this work in order to give an additional degree of freedom to the model. However, we can notice that it is in the same order of magnitude as  $\lambda_{air}$  and thus could be considered as a  $\lambda_{air}$  reference (in the same logic of  $P_{ref}$  for instance).

#### 4.2.2. Diffusion Limiting Current Density Model

Equation (9) is used for modeling the temperature dependency of  $j_{lim}$  in the literature [44]. This equation was used in [37] for modeling the 27  $j_{lim}$  obtained after the parameter identification described in Section 4.1.2 and the results were consistent (to perform this modeling, the parameters  $D_{eff,O_2}$  and  $\varphi$  were identified by fitting Equation (9) to the 27 previously obtained values of  $j_{lim}$  for each air over-stoichiometry  $\lambda_{air}$ ).

$$j_{lim} = \frac{nF}{\delta} D_{eff,O_2} \left( \frac{T}{T_{ref}} \right)^\varphi [O_2] \quad (9)$$

where  $\delta$  is the thickness of the cathodic gas diffusion layer, GDL (400  $\mu$ m),  $D_{eff}$  is the effective diffusion coefficient for oxygen (identified parameter),  $\varphi$  an empirical coefficient (identified

parameter), and  $[O_2]$  the oxygen concentration in the gas channels ( $4.47 \times 10^{-5} \text{ mol}\cdot\text{cm}^{-3}$  in normal conditions: 1 atm and  $0^\circ\text{C}$ , i.e., 273.15 K).

The air over-stoichiometry dependency is introduced in the model by correcting the oxygen concentration in the gas channels ( $[O_2]$ ) through adding two empiric coefficients (a constant,  $\lambda_{air,ref}$ , and a parameter to identify ( $\sigma$ ) in a logarithmic function as it is shown in Equation (10).

$$j_{lim} = \frac{nF}{\delta} D_{eff,O_2} \left( \frac{T}{T_{ref}} \right)^\varphi [O_2] \ln \left( \sigma \frac{\lambda_{air}}{\lambda_{air,ref}} \right) \quad (10)$$

where  $\delta$  is the thickness of the cathodic GDL (400  $\mu\text{m}$ ),  $D_{eff}$  is the effective diffusion coefficient for oxygen,  $\varphi$  an empirical coefficient and  $[O_2]$  the oxygen concentration in the gas channels ( $4.47 \times 10^{-5} \text{ mol}\cdot\text{cm}^{-3}$  in normal conditions: 1 atm and  $0^\circ\text{C}$ ).

The logarithmic dependency on  $\lambda_{air}$  was chosen after comparing the fitting of the 27  $j_{lim}$  as a function of  $\lambda_{air}$  by different trend curves (linear, power, and logarithmic) because it permits to obtain the best fit (result not shown here). The only parameters to identify for modelling 27  $j_{lim}$  are  $D_{eff,O_2}$ ,  $\varphi$ , and  $\sigma$ . This identification gives a global error of 3.38% and a maximum error (for one  $j_{lim}$ ) of 8.02%.

The parameter  $\varphi = 2.93$  is different from the values found in the literature for LT and HT-PEMFCs, but in the same order of magnitude: 1.75 [45], 1.5 [44,46], and 1.73 to 2.07 [47] (p. 67). The parameter  $\sigma = 4.16$  is not present in the literature; it was introduced in this work in order to give an additional degree of freedom to the model. The effective diffusion coefficient for oxygen ( $D_{eff,O_2}$ ) is equal to  $5.76 \times 10^{-3} \text{ cm}^2\cdot\text{s}^{-1}$  far from the value found in the literature: around  $1 \times 10^{-1} \text{ cm}^2\cdot\text{s}^{-1}$  in LT-PEMFCs and between  $1.2 \times 10^{-2} \text{ cm}^2\cdot\text{s}^{-1}$  and  $2.4 \times 10^{-1} \text{ cm}^2\cdot\text{s}^{-1}$  in HT-PEMFCs [33,48,49] with the few data found.

## 5. Model Validation

The air over-stoichiometry-dependent cell voltage model (simply called the “Final Model” in the following sections) is finally obtained by substituting Equations (8) and (10) into Equations (3) and (5), respectively. This model uses only nine parameters, whatever the number of experimental curves to model. The validity of this model will be studied in two steps. First, the accuracy obtained by parameter identification on the 27 experimental polarization curves will be discussed. Second, the ability to model curves that were not used to identify the parameter will be investigated (performance prediction capacity).

### 5.1. Final Model Accuracy

With the Final Model, the 27 polarization curves are now modeled by only 9 parameters, namely,  $\alpha$ ,  $\gamma$ ,  $E_a$ ,  $i_{0,ref}$ ,  $coef_{\lambda_{air}}$ ,  $\beta$ ,  $D_{eff}$ ,  $\varphi$ , and  $\sigma$ . The identification process applied simultaneously to the 27 curves with the Final Model gives an overall error of 1.42%, and the maximum error at a given current level is about 18%, which corresponds to the curve at  $140^\circ\text{C} - \lambda_{H_2/air} = 1.35/1.5$ . It must be noted that this curve shows unusual performance compared to the ones obtained at the same temperature but with different  $\lambda_{H_2}$ . Thus, this “anomaly” is imputed to reversible losses that we were unable to clarify (the next day of the test, the cell recovers normal performance). Then, the second worst error obtained is equal to 15% and corresponds to the curve at  $140^\circ\text{C} - \lambda_{H_2/air} = 1.2/1.5$  (see Figure 6), which shows much more consistency performance than the “anomaly” curve at  $140^\circ\text{C} - \lambda_{H_2/air} = 1.35/1.5$ . The global error was doubled compared to the one obtained with the Basic Model (0.72%), and the maximum error was only 2.55% with the Basic Model. However, the Final Model needs six times fewer parameters to identify, and all of them are common to the complete OC domain explored with a much better dependence on OCs (the values of the identified parameters are given in Table 3).

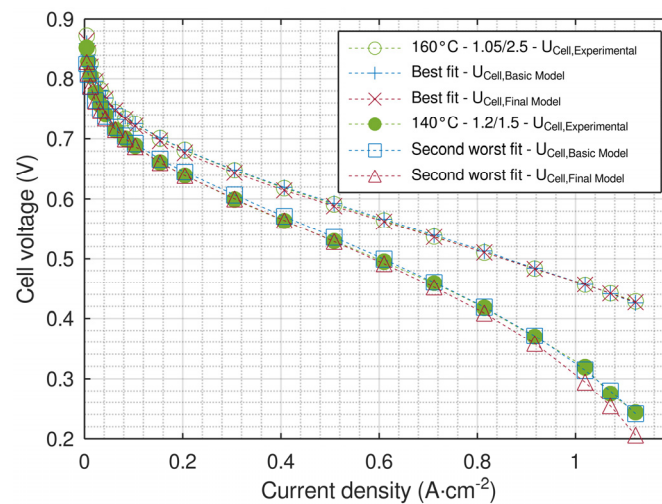


**Figure 6.** Experimental (o, ●, and green) and modeled cell voltages with the Basic Model (+, □ and blue) and the Final Model (x, Δ and red) for the best (160 °C –  $\lambda_{H2/air} = 1.05/2.5$ ) and second worst (140 °C –  $\lambda_{H2/air} = 1.2/1.5$ ) fit.

**Table 3.** Values of identified parameters and modeling errors.

Quantity	Identification on 27 VI (Presented in Section 5.1)	Identification on 27 Corrected VI	Identification on 9 VI (Presented in Section 5.2)	Identification on 9 Corrected VI
Global Error (%)	1.42	1.05	1.46	1.09
Maximum Error (%)	18	16.48	29.84	27.27
$\alpha$	0.46	0.48	0.47	0.48
$\gamma$	0.47	0.20	0.44	0.14
$E_a$ (J·mol <sup>-1</sup> )	$8.42 \times 10^4$	$8.23 \times 10^4$	$8.59 \times 10^4$	$8.16 \times 10^4$
$i_{0,ref}$ (A)	$5.62 \times 10^{-4}$	$2.29 \times 10^{-4}$	$6.61 \times 10^{-4}$	$9.96 \times 10^{-5}$
$coef_{\lambda_{air}}$	3.6	2.34	6.98	0.01
$\beta$	0.11	0.12	0.10	0.12
$D_{eff}$	$5.61 \times 10^{-3}$	$5.19 \times 10^{-3}$	$5.68 \times 10^{-3}$	$5.25 \times 10^{-3}$
$\varphi$	1.97	1.95	1.76	1.75
$\sigma$	4.32	4.56	4.37	4.55

Figure 6 shows the experimental curves at 160 °C –  $\lambda_{H2/air} = 1.05/2.5$  (best fit) and 140 °C –  $\lambda_{H2/air} = 1.2/1.5$  (second worst fit) modeled with the Basic Model and the Final Model. It can be observed that both models underestimate the voltage. At high current densities (i.e., higher than 0.8 A·cm<sup>-2</sup>), the Final Model shows a significantly higher error. Furthermore, it must be noticed that the error is usually maximum at high or low current densities. However, it is not recommended to use a HT-PEMFC at these ranges of current densities (low and high voltage) in order to limit MEA degradations [12,33].

The parameters  $\alpha = 0.46$  and  $\gamma = 0.47$  are very close to the ones obtained in Section 4.2.1) and [50] and  $\beta = 0.11$  is identical with the identified one presented in Section 4.2.2), and thus, consistent with the literature. Parameters  $E_a$ ,  $i_{0,ref}$ ,  $D_{eff}$  and  $coef_{\lambda_{air}}$  are in the same order of magnitude as the ones obtained in Sections 4.2.1 and 4.2.2 (see Table 3).

It has to be noticed that  $coef_{\lambda_{air}}$  is closed to 2 in this last identification using the Final Model. Consequently, another identification was made by fixing  $coef_{\lambda_{air}}$  to 2 (as the  $\lambda_{air,ref}$  parameter is not to be identified anymore) and  $\gamma$  to 0.5 (according to the literature [41,42]). This identification with only 7 parameters to identify ( $\alpha$ ,  $E_a$ ,  $i_{O,ref}$ ,  $\beta$ ,  $D_{eff}$ ,  $\varphi$ , and  $\sigma$ ) induce a

similar accuracy (global error of 1.41% and maximum error of 18.27%) with a 22% parameter number reduction and very closed values obtained for the left parameters.

One should note that the Final Model presents an interesting fit for both linear and logarithmic curve shapes at high current densities. This is not trivial to obtain by modeling because some parameters are correlated, as  $\beta$  and  $j_{lim}$  for instance (a small  $\beta$  can compensate a high  $j_{lim}$ ). Here, the multicurve approach associated with a  $\lambda_{air}$  dependent model seems to be promising for parameter separation of the three physicochemical phenomena involved, reducing the multimodality of the problem.

### 5.2. Performance Prediction Capacity

In order to study the performance prediction ability of the model, we will briefly use the theory of Design of Experiment (DoE). In fact, the sensibility study presented in Table 1 can be considered a full factorial design with 3 factors and 3 levels for each (see Figure 7). The 27 OCs tested are represented with circles (red or green) in Figure 7. A Latin square, corresponding to 9 OCs, was used as a “learning area” to identify model parameters on the corresponding polarization curves (red circles). Then, the other 18 curves (green circles) have been estimated with the obtained parameters from the 9 curve fitting. After that, the accuracy of the model on the 27 curves (which are known experimentally) was calculated. Thus, as in the previous section, we obtained an overall error on 27 curves, but here the model parameters were identified only on 9 curves.

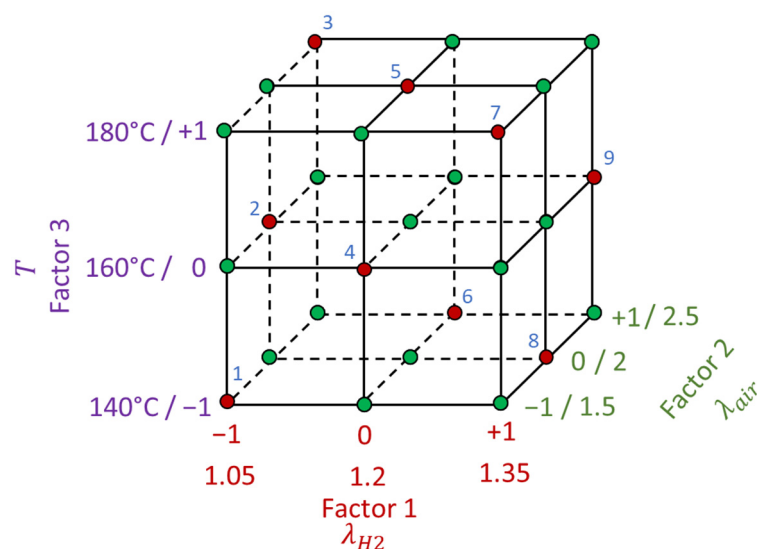


**Figure 7.** Illustration of a full factorial design (red and green circles) and a Latin square (red circles) applied to the sensibility study.

However, the modeling of the 18 curves not used as “learning areas” requires rigorously knowing the value of  $R_{cell}$  (in ohmic losses, see Equation (4)) for each curve. In order to simplify the problem, we have considered that the  $R_{cell}$  is only temperature and current dependent (not over-stoichiometry dependent). Furthermore, it has been verified (results are not shown here) that the use of only one value of  $R_{cell}$  per temperature does not significantly reduce the accuracy (the global error is still 1.42% as in the previous identification; see Section 5.1). Then, in order to model the 18 “other” curves, we will use the  $R_{cell}$  from the 9 curves used for fitting and consider it constant per temperature but dependent on current.

The identification process was applied simultaneously to the 9 curves with the Final Model (see Figure 8). It gives an overall error on 27 curves of 1.46%, and the maximum error at a given current level is about 30%, and it corresponds to the “anomaly” curve at 140 °C –  $\lambda_{H2/air} = 1.35/1.5$  (see Section 5.1). The second worst accuracy obtained is equal to 7%, and it corresponds to the curve at 140 °C –  $\lambda_{H2/air} = 1.2/1.5$  (compared to

15% with the full design). Thus, removing the “anomaly” curve from the data used for identification seems to increase the model accuracy on the left 140 °C curves. In fact, the “anomaly” curve could perturb the identification by introducing uncommon data behavior to the problem. Finally, the model “trained” on 9 curves is globally 2.8% less accurate than the identification on 27 curves (see Section 5.1). However, three times fewer curves have been used to identify the model parameters, which is very encouraging in order to simultaneously reduce the number of experiments and obtain interesting accuracy (the values of the identified parameters are given in Table 3).

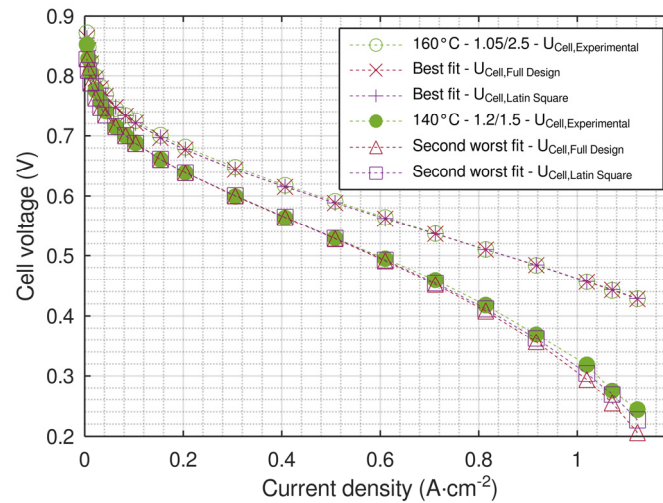


**Figure 8.** Experimental (o, •, and green) and modeled cell voltages with the Final Model using the full factorial design (27 curves) for parameter identification (x, Δ, and red) and the Latin square design (9 curves) for parameter identification (+, □, and purple) for the best (160 °C –  $\lambda_{H_2/air} = 1.05/2.5$ ) and second worst (140 °C –  $\lambda_{H_2/air} = 1.2/1.5$ ) fit.

### 5.3. Impact of Cell Voltage Degradation

The MEAs experienced voltage degradation during the sensibility study, which has been monitored by acquiring a reference VI curve at nominal conditions between each of the 27 VI curves of the sensibility study (see Section 2 for more details). In the following, a VI curve of the sensibility study will be called a SS-VI curve.

The voltage of each SS-VI curve at a given current density  $j$  has been corrected thanks to the voltage degradation measured between the two consecutive reference VI curves surrounding a given SS-VI curve with the following equation:

$$U_{cell}^{corrected}(j) = U_{cell}(j) \times \left(1 + \frac{RD(j)}{100}\right) \quad (11)$$

were  $U_{cell}^{corrected}$  states for the cell voltage of the SS-VI curve corrected by the voltage degradation measured,  $U_{cell}$  states for the cell voltage of the SS-VI curve,  $RD$  states for the relative difference between the two consecutive reference VI curves surrounding the SS-VI curve:

$$RD(j) = 100 \times \left(\frac{U_{after}^{ref}(j) - U_{before}^{ref}(j)}{U_{before}^{ref}(j)}\right) \quad (12)$$

were  $U_{before}^{ref}$  and  $U_{after}^{ref}$  are the measured voltages of the reference VI curves, respectively, before and after the considered SS-VI curve.

Furthermore, the total cell resistance increases during the test. A difference of 2.8 mΩ·cm<sup>2</sup> in the cell resistance was measured by EIS at 1.1 A·cm<sup>−2</sup> between the beginning and the end of the sensibility study. This difference leads to a maximum voltage loss of 3 mV at 1.1 A·cm<sup>−2</sup>. This loss of voltage was not taken into account in the following part of this work. Then, the voltage is corrected for each VI, but not the measure of the total resistance of the cell.

Figure 9 shows the first and last *reference VI curves* obtained during the whole campaign. One can see that the maximum relative difference is around 7.25% at  $1.08 \text{ A}\cdot\text{cm}^{-2}$  which corresponds to 8 mV and so a degradation rate of approximately  $38 \mu\text{V}\cdot\text{h}^{-1}$ . Typical degradation rates of around  $4.5 \mu\text{V}\cdot\text{h}^{-1}$  have been reported for BASF MEAs at a constant current of  $0.2 \text{ A}\cdot\text{cm}^{-2}$  [33]. This means that the sensibility study has a significant impact on the aging of the cell. It therefore seems even more important to seek to minimize the number of tests while maintaining the correct accuracy of the model, as we sought to do with the approach presented in the previous section.

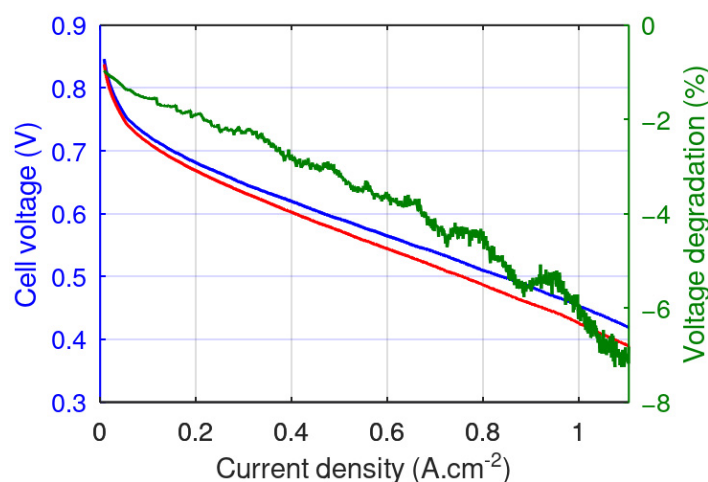


**Figure 9.** First (blue and left axis) and last (red and left axis) reference VI curves obtained and associated relative difference (green and right axis).

Two parametric identifications, with the Final model, have been carried out on the *corrected VI curves*: (i) an identification using all 27 corrected VI (in the same spirit of the identification presented in Section 5.1) and (ii) an identification using only 9 VI curves (in the same spirit of the identification presented in Section 5.2 with the Latin square factorial design).

Table 3 presents some results and parameter values for each parametric identification. One can see that all the identified parameters have the same order of magnitude compared to the identification without voltage correction. The global error is even better after voltage correction. A possible explanation could be the fact that trying to obtain a good fit on some degraded curve can lead to the identification of unsuitable global parameters. Unfortunately, the value of the reaction order  $\gamma$  is much lower with the corrected voltage and far from its theoretical value of 0.5.

In view of these results, it appears to the authors that the degradation of the cell during the tests does not refute the multi-VI method developed during this work or the relative validity of the model under the conditions considered.

However, these results do not prove the relevance of this voltage correction method. Indeed, the reference VI curves are obtained with a slope instead of the current stage in the case of the SS-VI curve. Then, the steady-state regime is not reached in the case of reference VI curves, which could lead to different voltage values. Also, the variation of the ohmic resistance was not considered in this correction.

## 6. Conclusions

The sensibility study of 27 OCs tested permits the evaluation of the most preponderant OCs impacting the cell voltage in steady-state operation: the temperature and the air over-stoichiometry.

A first model (called the Basic Model) was developed, allowing us to obtain very satisfying results on the curves obtained during the sensibility study with a model initially developed for LT-PEMFC. In order to be able to predict the performance of the cell in a

given OC, the model was improved based on the hypothesis that the impact of hydrogen over-stoichiometry is negligible compared to the impact of temperature and air over-stoichiometry. The main originality of this model is to consider the impact of air over-stoichiometry simultaneously at “low current density” and “high current density.” First, with a simple analytical model of  $j_0$  where a correction of the partial pressure of oxygen in the channels permits to estimate the partial pressure at active sites (i.e., in the catalyst layer). The air over-stoichiometry impact at “high current density” is considered in the calculation of  $j_{lim}$ . The simplicity of this 0D model allows for fast results and saves computation time, which can be useful in optimizing sizing, for example.

The so-called Final Model obtained used 6 times fewer parameters in order to model the 27 curves, and this number is independent of the quantity of curves to model. However, the global accuracy was divided by 2 compared to the Basic Model, which is still satisfying for an industrial application working between 0.2 and 0.8 A·cm<sup>-2</sup> for example. In fact, in order to maximize the cell lifetime, it is recommended to avoid low and high voltages (i.e., high and low current density, respectively) in HT-PEMFCs [12,33]. Also, fixing  $\alpha$  and  $\gamma$  (22% reduction in parameter number) permits obtaining the same accuracy and similar parameter values. Parameter values seem to be consistent with the literature, even if there are few of them in the literature on HT-PEMFC at present.

The predictability of the model was also validated in the domain explored during the sensibility study. The model shows remarkable accuracy on 27 curves by using only 9 curves to identify the parameters. The error was 2.8% higher than with the “training” on 27 curves, but 3 times fewer curves were used in order to identify the model parameters. This result is one of the main contributions of this work because it is quite encouraging for an industrial application in order to reduce the number of experiments and the cost of model development.

Furthermore, the proposed “multi-VI” approach with only one set of parameters seems to be an interesting way to converge towards the uniqueness of consistent parameters. In fact, some of the parameters of the Basic Model are strongly correlated, like the couples  $j_0/\alpha$  or  $j_{lim}/\beta$  which can disturb parameter consistency. In the approach presented here,  $\alpha$  and  $\beta$  are forced to be common to all the curves, which permits partially uncorrelated them to  $j_0$  and  $j_{lim}$  respectively.

It was also observed that there was a negligible variation in the total resistance of the cell measured by EIS ( $R_{cell}$ ) with COs (except with temperature), which allows for easy prediction of the voltage in untested COs.

In future work, it would be interesting to consider the hydrogen over-stoichiometry in the model in order to be more generic with over-type HT-PEM cells where it could be non-negligible. Furthermore, this work gives an interesting way to model the impact of the over-stoichiometry with relatively simple equations (i.e., a 0D model with no fluid dynamics computation), which seems to be much more difficult to perform with LT-PEMFC technology. However, this work does not provide a better understanding of the underlying mechanism that would explain the significant impact of the oxygen over-stoichiometry that is observed with an HT-PEMFC.

It must be noticed that the HT-PEMFC technology shows remarkable stability even under low gas over-stoichiometry. This is an advantage for improving modeling compared to LT-PEMFC. Also, this could facilitate the production of oxygen-depleted air, which can be used to inert the fuel tank of an aircraft. With the advantages of the HT-PEMFCs presented in the introduction, this technology can be interesting for a particular application, such as aeronautic transport, where both weight and volume are critical.

**Author Contributions:** Conceptualization, S.R., A.J. and C.T.; methodology, S.R., A.J. and C.T.; software, S.R.; validation, A.J., C.T., T.H., J.-B.J. and P.K.; writing—original draft preparation, S.R. and A.J.; writing—review and editing, A.J. and C.T.; supervision, A.J. and C.T. All authors have read and agreed to the published version of the manuscript.



**Funding:** The work was supported by IRT Saint Exupéry, SAFRAN, AIRBUS, the LAPLACE laboratory, and all the public funders (FEDER, Occitanie Region, French Government, and Toulouse Metropole) of the LAPLACE Hydrogen Platform, Toulouse, used for all tests during the FUCHYA project.

**Data Availability Statement:** The data presented in this study are available on request from the corresponding author. The data are not publicly available due to privacy.

**Acknowledgments:** The authors would like to express their sincere thanks to all the members of the FUCHYA project, namely the IRT Saint Exupéry, SAFRAN, AIRBUS, the LAPLACE laboratory, and the ANR (Agence Nationale de la Recherche). The authors would also like to thank all the public funders (FEDER, Occitanie Region, French Government, and Toulouse Metropole) of the LAPLACE, Hydrogen Platform, Toulouse, used for all tests during the FUCHYA project.

**Conflicts of Interest:** Author Théophile Horde was employed by the company Airbus. Author Jean-Baptiste Jollys was employed by the company Alstom. The remaining authors declare that the research was conducted in the absence of any commercial or financial relationships that could be construed as a potential conflict of interest.

## References

- Derwent, R.; Simmonds, P.; O'Doherty, S.; Manning, A.; Collins, W.; Stevenson, D. Global environmental impacts of the hydrogen economy. *Int. J. Nucl. Hydrog. Prod. Appl.* **2006**, *1*, 57. [CrossRef]
- Lee, D.S.; Fahey, D.W.; Skowron, A.; Allen, M.R.; Burkhardt, U.; Chen, Q.; Doherty, S.J.; Freeman, S.; Forster, P.M.; Fuglestvedt, J.; et al. The contribution of global aviation to anthropogenic climate forcing for 2000 to 2018. *Atmos. Environ.* **2021**, *244*, 117834. [CrossRef] [PubMed]
- Li, Q.; He, R.; Jensen, J.; Bjerrum, N. PBI-Based Polymer Membranes for High Temperature Fuel Cells—Preparation, Characterization and Fuel Cell Demonstration. *Fuel Cells* **2004**, *4*, 147–159. [CrossRef]
- Lim, J.W.; Kim, M.; Yu, Y.H.; Lee, D.G. Development of Carbon/PEEK Composite Bipolar Plates with Nano-Conductive Particles for High-Temperature PEM Fuel Cells (HT-PEMFCs). *Compos. Struct.* **2014**, *118*, 519–527. [CrossRef]
- Gang, X.; Qingfeng, L.; Hjuler, H.A.; Bjerrum, N.J. Hydrogen Oxidation on Gas Diffusion Electrodes for Phosphoric Acid Fuel Cells in the Presence of Carbon Monoxide and Oxygen. *J. Electrochem. Soc.* **1995**, *142*, 2890–2893. [CrossRef]
- Kösters, T.L.; Liu, X.; Kožulović, D.; Wang, S.; Friedrichs, J.; Gao, X. Comparison of phase-change-heat-pump cooling and liquid cooling for PEM fuel cells for MW-level aviation propulsion. *Int. J. Hydrogen Energy* **2022**, *47*, 29399–29412. [CrossRef]
- Kösters, T.L.; von Schweinitz, A.G.; Heere, M.; Friedrichs, J.; Gao, X. Experimental study and simulations of hydrogen cooling effectiveness for aviation PEM fuel cells. *Nature Sci. Rep.* **2023**, *13*, 23016. [CrossRef]
- Composite Bipolar Plates Datasheet. 2023. Available online: [www.hycco.fr](http://www.hycco.fr) (accessed on 10 November 2023).
- Cheng, X.; Zhang, J.; Tang, Y.; Song, C.; Shen, J.; Song, D.; Zhang, J. Hydrogen crossover in high-temperature PEM fuel cells. *J. Power Sources* **2007**, *167*, 25–31. [CrossRef]
- Sood, R. Electrolytes Polymère Nano-Structurés à Base de Liquides Ioniques Pour les Piles à Combustible Hautes Températures. Ph.D. Thesis, Université de Grenoble, Grenoble, France, 2012.
- Chandan, A.; Hattenberger, M.; El-kharouf, A.; Du, S.; Dhir, A.; Self, V.; Pollet, B.G.; Ingram, A.; Bujalski, W. High temperature (HT) polymer electrolyte membrane fuel cells (PEMFC)—A review. *J. Power Sources* **2013**, *231*, 264–278. [CrossRef]
- Schmidt, T.J.; Baurmeister, J. Properties of high-temperature PEFC Celtec®-P 1000 MEAs in start/stop operation mode. *J. Power Sources* **2008**, *176*, 428–434. [CrossRef]
- Hartnig, C.; Schmidt, T.J. Simulated start–stop as a rapid aging tool for polymer electrolyte fuel cell electrodes. *J. Power Sources* **2011**, *196*, 5564–5572. [CrossRef]
- Büchi, F.N.; Inaba, M.; Schmidt, T.J. (Eds.) High-Temperature Polymer Electrolyte Fuel Cells: Durability Insights. In *Polymer Electrolyte Fuel Cell Durability*; Springer: New York, NY, USA, 2009; pp. 199–221.
- Kazula, S.; de Graaf, S.; Enghardt, L. Review of fuel cell technologies and evaluation of their potential and challenges for electrified propulsion systems in commercial aviation. *J. Glob. Power Propuls. Soc.* **2023**, *7*, 43–57. [CrossRef]
- Tang, H.; Geng, K.; Wu, L.; Liu, J.; Chen, Z.; You, W.; Li, N. Fuel cells with an operational range of  $-20^{\circ}\text{C}$  to  $200^{\circ}\text{C}$  enabled by phosphoric acid-doped intrinsically ultramicroporous membranes. *Nat. Energy* **2022**, *7*, 153–162. [CrossRef]
- Mohamed, B.; Ali, B.; Ammar, N.; Salah, L.; Nordine, S.; Ahmed, B. Contribution and investigation to compare models parameters of (PEMFC), comprehensives review of fuel cell models and their degradation. *Energy* **2019**, *168*, 182–199.
- Abdul Rasheed, R.K.; Liao, Q.; Caizhi, Z.; Chan, S.H. A review on modelling of high temperature proton exchange membrane fuel cells (HT-PEMFCs). *Int. J. Hydrogen Energy* **2017**, *42*, 3142–3165. [CrossRef]
- Kulikovskiy, A.A. The effect of stoichiometric ratio  $\lambda$  on the performance of a polymer electrolyte fuel cell. *Electrochim. Acta* **2004**, *49*, 617–625. [CrossRef]
- Ramos-Paja, C.; Giral, R.; Martinez-Salamero, L.; Romano, J.; Romero, A.; Spagnuolo, G. A PEM fuel-cell model featuring oxygen-excess-ratio estimation and power-electronics interaction. *IEEE Trans. Ind. Electron.* **2010**, *57*, 1914–1924. [CrossRef]

21. Pukrushpan, J.T.; Stefanopoulou, A.G.; Peng, H. Control of fuel cell breathing. *IEEE Control Syst. Mag.* **2004**, *24*, 30–46.
22. Liu, J.; Gao, Y.; Su, X.; Wack, M.; Wu, L. Disturbance-observer-based control for air management of PEM fuel cell systems via sliding mode technique. *IEEE Trans. Control Syst. Technol.* **2018**, *27*, 1129–1138. [[CrossRef](#)]
23. Liu, J.; Laghrouche, S.; Ahmed, F.; Wack, M. PEM fuel cell air-feed system observer design for automotive applications: An adaptive numerical differentiation approach. *Int. J. Hydrogen Energy* **2014**, *39*, 17210–17221. [[CrossRef](#)]
24. Deng, H.; Li, Q.; Chen, W.; Zhang, G. High-Order Sliding Mode Observer Based OER Control for PEM Fuel Cell Air-Feed System. *IEEE Trans. Energy Convers.* **2018**, *33*, 232–244. [[CrossRef](#)]
25. Yuan, H.; Dai, H.F.; Wei, X.Z.; Ming, P.W. Model-based observers for internal states estimation and control of proton exchange membrane fuel cell system: A review. *J. Power Sources* **2020**, *468*, 228376. [[CrossRef](#)]
26. In-Su, H.; Chang-Bock, C. Performance prediction and analysis of a PEM fuel cell operating on pure oxygen using data-driven models: A comparison of artificial neural network and support vector machine. *Int. J. Hydrogen Energy* **2016**, *41*, 10202–10211.
27. Sisworahardjo, N.S.; Yalcinoz, T.; El-Sharkh, M.Y.; Alam, M.S. Neural network model of 100 W portable PEM fuel cell and experimental verification. *Int. J. Hydrogen Energy* **2010**, *35*, 9104–9109. [[CrossRef](#)]
28. Ziogou, C.; Voutetakis, S.; Georgiadis, M.C.; Papadopoulou, S. Model predictive control (MPC) strategies for PEM fuel cell systems—A comparative experimental demonstration. *Chem. Eng. Res. Des.* **2018**, *131*, 656–670. [[CrossRef](#)]
29. Wang, X.C.; Chen, J.Z.; Quan, S.W.; Wang, Y.X.; He, H.W. Hierarchical model predictive control via deep learning vehicle speed predictions for oxygen stoichiometry regulation of fuel cells. *Appl. Energy* **2020**, *276*, 115460. [[CrossRef](#)]
30. Lan, H.; Yang, L.; Zheng, F.; Zong, C.; Wu, S.; Song, X. Analysis and optimization of high temperature proton exchange membrane (HT-PEM) fuel cell based on surrogate model. *Int. J. Hydrogen Energy* **2020**, *45*, 12501–12513. [[CrossRef](#)]
31. Berna, S.; Dilara, G.C.; Yilser, D.; Thomas, S.; Inci, E. Modeling and sensitivity analysis of high temperature PEM fuel cells by using Comsol Multiphysics. *Int. J. Hydrogen Energy* **2016**, *41*, 10001–10009.
32. Dilara, G.C.; Berna, S.; Yilser, D.; Inci, E. Three-dimensional modeling of a high temperature polymer electrolyte membrane fuel cell at different operation temperatures. *Int. J. Hydrogen Energy* **2016**, *41*, 10060–10070.
33. Rigal, S.; Turpin, C.; Jaafar, A.; Hordé, T.; Jollys, J.-B.; Chadourne, N. Ageing tests at constant currents and associated modeling of high temperature PEMFC MEAs. *Fuel Cells* **2020**, *20*, 272–284. [[CrossRef](#)]
34. Baudy, M.; Jaafar, A.; Turpin, C.; Abbou, S.; Rigal, S. Experimental study of the potential degradation due to the polarization curve of a high temperature proton exchange membrane fuel cell. *Int. J. Hydrogen Energy* **2022**, *48*, 20945–20956. [[CrossRef](#)]
35. Fontès, G.; Turpin, C.; Saisset, R.; Meynard, T.; Astier, S. Interactions Between Fuel Cells and Power Converters: Influence of Current Harmonics on a Fuel Cell Stack. *IEEE Trans. Power Electron.* **2007**, *22*, 670–678. [[CrossRef](#)]
36. Labach, I.; Rallières, O.; Turpin, C. Steady state Semi-empirical Model of a Single Proton Exchange Membrane Fuel Cell (PEMFC) at Varying Operating Conditions. *Fuel Cells* **2017**, *17*, 166–177. [[CrossRef](#)]
37. Rigal, S.; Turpin, C.; Jaafar, A.; Chadourne, N.; Hordé, T.; Jollys, J.-B. Steady-state modelling of a HT-PEMFC under various operating conditions. In Proceedings of the 2019 IEEE 12th International Symposium on Diagnostics for Electrical Machines, Power Electronics and Drives (SDEMPED), Toulouse, France, 27–30 August 2019; pp. 439–445.
38. Qi, Z.; Buelte, S. Effect of open circuit voltage on performance and degradation of high temperature PBI–H3PO4 fuel cells. *J. Power Sources* **2006**, *161*, 1126–1132. [[CrossRef](#)]
39. Kim, J.; Kim, M.; Kang, T.; Sohn, Y.J.; Song, T.; Choi, K.H. Degradation modeling and operational optimization for improving the lifetime of high-temperature PEM (proton exchange membrane) fuel cells. *Energy* **2014**, *66*, 41–49. [[CrossRef](#)]
40. Labach, I. Caractérisation et Modélisation de Piles à Combustible et D'électrolyseurs PEM a Conditions Opératoires Variables en Vue de Leur Association. Ph.D. Thesis, Université de Toulouse, Toulouse, France, 2016.
41. Neyerlin, K.C.; Gu, W.; Jorne, J.; Gasteiger, H.A. Determination of Catalyst Unique Parameters for the Oxygen Reduction Reaction in a PEMFC. *J. Electrochem. Soc.* **2006**, *153*, 1955–1963. [[CrossRef](#)]
42. Subramanian, N.P.; Greszler, T.A.; Zhang, J.; Gu, W.; Makharia, R. Pt-Oxide Coverage-Dependent Oxygen Reduction Reaction (ORR) Kinetics. *J. Electrochem. Soc.* **2012**, *159*, 531–540. [[CrossRef](#)]
43. Jinyi, L.; Yongkang, J.; Xiaosong, Z.; Lirong, F.; Meilong, D. Performance optimization of an HT-PEMFC and PSA integrated system with impure hydrogen containing CO<sub>2</sub>. *Appl. Therm. Eng.* **2022**, *214*, 118859.
44. Wang, Y.; Feng, X. Analysis of the Reaction Rates in the Cathode Electrode of Polymer Electrolyte Fuel Cells II. Dual-Layer Electrodes. *J. Electrochem. Soc.* **2009**, *156*, B403–B409. [[CrossRef](#)]
45. Chippar, P.; Ju, H. Numerical modeling and investigation of gas crossover effects in high temperature proton exchange membrane (PEM) fuel cells. *Int. J. Hydrogen Energy* **2013**, *38*, 7704–7714. [[CrossRef](#)]
46. Park, J.; Min, K. A quasi-three-dimensional non-isothermal dynamic model of a high-temperature proton exchange membrane fuel cell. *J. Power Sources* **2012**, *216*, 152–161. [[CrossRef](#)]
47. Vang, J.R. HTPeM Fuel Cell Impedance: Mechanistic Modelling and Experimental Characterisation. Ph.D. Thesis, Aalborg University, Aalborg, Denmark, 2014.
48. Kim, M.; Kang, T.; Kim, J.; Sohn, Y.J. One-dimensional modeling and analysis for performance degradation of high temperature proton exchange high fuel cell using PA doped PBI membrane. *Solid State Ion.* **2014**, *262*, 319–323. [[CrossRef](#)]

49. Hu, J.; Zhai, Y.; Liu, G.; Hu, J.; Yi, B. Performance degradation studies on PBI/H<sub>3</sub>PO<sub>4</sub> high temperature PEMFC and one-dimensional numerical analysis. *Electrochim. Acta* **2006**, *52*, 394–401. [[CrossRef](#)]
50. Jo, A.; Oh, K.; Lee, J.; Han, D.; Kim, D.; Kim, J.; Kim, B.; Kim, J.; Park, D.; Kim, M.; et al. Modeling and Analysis of a 5 KWe HT-PEMFC System for Residential Heat and Power Generation. *Int. J. Hydrogen Energy* **2017**, *42*, 1698–1714. [[CrossRef](#)]

**Disclaimer/Publisher’s Note:** The statements, opinions and data contained in all publications are solely those of the individual author(s) and contributor(s) and not of MDPI and/or the editor(s). MDPI and/or the editor(s) disclaim responsibility for any injury to people or property resulting from any ideas, methods, instructions or products referred to in the content.